
PSO-PINN: PHYSICS-INFORMED NEURAL NETWORKS TRAINED WITH PARTICLE SWARM OPTIMIZATION

Caio Davi **Ulisses Braga Neto**
Department of Electrical and Computer Engineering
Texas A&M University
College Station, TX 77843 USA
{caio.davi,ulisses}@tamu.edu

July 19, 2022

ABSTRACT

Physics-informed neural networks (PINNs) have recently emerged as a promising application of deep learning in a wide range of engineering and scientific problems based on partial differential equation models. However, evidence shows that PINN training by gradient descent displays pathologies and stiffness in gradient flow dynamics. In this paper, we propose the use of a hybrid particle swarm optimization and gradient descent approach to train PINNs. The resulting PSO-PINN algorithm not only mitigates the undesired behaviors of PINNs trained with standard gradient descent but also presents an ensemble approach to PINN that affords the possibility of robust predictions with quantified uncertainty. Experiments with linear and nonlinear PDE models demonstrate the efficacy of the proposed methodology.

1 Introduction

Physics-informed machine learning is an emerging area that promises to have a profound and lasting impact in science and engineering. Physics-informed neural networks (PINNs) [1], in particular, have shown remarkable success in a variety of problems modeled by partial differential equations [2, 3]. PINNs exploit the universal approximation capabilities of neural networks[4]. Unlike traditional neural networks, PINNs employ a multi-part loss function containing data-fitting and PDE residual components. And differently from traditional numerical methods, PINNs are meshless, producing a solution over an entire, possibly irregular, domain, rather than on a pre-specified grid of points.

Standard gradient descent tools already in widespread use for training deep neural networks, such as stochastic gradient [5] and ADAM [6], were promptly adopted as the methods of choice to train PINN. However, an accumulating body of evidence shows that gradient descent exhibits pathological behavior when training PINNs, especially when the differential equation solution contains high-frequencies [7, 8]. Numerous approaches have been proposed to mitigate this undesirable behavior, including weighting the loss function [8, 9, 10], domain decomposition[11, 12], and changes to the neural network architecture [7]. Recent work attributed this behavior to stiffness in the gradient flow dynamics of the PINNs loss functions, which leads to unstable convergence for gradient-based optimization algorithms [7, 8].

In this work, we propose the use of deep neural network ensembles as predictive models combining the predictions from two or more other models. One of the main reasons behind the success of ensemble methods is increasing the diversity among the base classifiers [13], thus reducing the variance on the final predictor. Although there are reports from three decades ago [14] demonstrating that neural network ensembles are capable of reducing the generalization error, it is still a major topic in several fields of applications [15, 16, 17], including PINNs [18].

Particle Swarm Optimization (PSO) [19] is a metaheuristic optimization algorithm used in numerous applications, including deep neural network training [20, 21, 22, 23, 24]. Indeed, the original paper on PSO by Kennedy and Eberhart was motivated in part by neural network training. In this paper, we propose to investigate the use of a PSO-based algorithm as an alternative to purely derivative-based methods to train PINNs. The resulting PSO-PINN algorithm not only mitigates the pathologies associated with gradient-based optimization, but also produces a diverse ensemble of trained neural networks, which enables the application of ensemble methods to PINNs, such as uncertainty quantification[25] and variance reduction[26].

To our knowledge, PSO-PINN is the first algorithm for training PINNs based on swarm optimization. PSO-PINN is based on the PSO-BP algorithm [27], a technique originally proposed for training traditional neural networks. PSO-BP is a hybrid technique that combines particle swarm optimization and gradient descent, using the gradient as one of the components in the particle velocity vector (see Section 2.3 for details).

Experimental results with several ODE and PDE benchmarks show that PSO-PINN consistently outperforms a baseline PINN trained with Adam gradient descent in diverse scenarios. These results also demonstrate the capability of PSO-PINN ensembles in uncertainty quantification.

This paper is organized as follows. Section 2 provides a brief overview of deep neural networks, physics-informed neural networks, and particle swarm optimization, whereas Section 3 describes in detail the PSO-PINN algorithm. Section 4 presents experimental results using various ODE and PDE benchmarks. Section 6 provides concluding remarks and future directions.

2 Background

In this section, we define deep neural networks, then introduce physics-informed deep neural networks, and finally describe the PSO-BP method.

2.1 Deep Neural Networks

The feed-forward fully-connected neural network is the basic architecture used in deep learning algorithms[28]. A fully-connected neural network with L layers is a function $f_\theta : \mathbb{R}^d \rightarrow \mathbb{R}^k$ described by

$$f_\theta(x) = W^{[L-1]}\sigma \circ (\dots \circ (W^{[0]}x + b^{[0]}) + \dots) + b^{[L-1]} \quad (1)$$

where σ is an entry-wise activation function, $W^{[l]}$ and $b^{[l]}$ are respectively the weight matrices and the bias corresponding to each layer l , and θ is the set of weights and biases:

$$\theta = (W^{[0]}, \dots, W^{[L-1]}, b^{[0]}, \dots, b^{[L-1]}). \quad (2)$$

Among popular choices for the activation function are the sigmoid function, the hyperbolic tangent function (tanh), and the rectified linear unit (ReLU) [29]. To fit the neural network $f_\theta(x)$ to data, one minimizes a suitable loss function. A popular choice in traditional deep learning is the mean square error(MSE):

$$\mathcal{L} = |f_\theta(x) - y|^2, \quad (3)$$

where $y \in \mathbb{R}^k$ is the target value.

2.2 Physics-Informed Neural Networks

Consider a non-linear differential equation of the general form:

$$\begin{aligned} \mathcal{N}[u(\mathbf{x})] &= g(\mathbf{x}), & \mathbf{x} \in \Omega, \\ u(\mathbf{x}s) &= h(\mathbf{x}), & \mathbf{x} \in \partial\Omega, \end{aligned} \quad (4)$$

where $\Omega \subset \mathbb{R}^d$, $u : \Omega \rightarrow \mathbb{R}^k$, and $\mathcal{N}[\cdot]$ is a differential operator. We employ a neural network $f_\theta(x)$ to approximate the unknown $u(x)$, using the loss function

$$\mathcal{L}_r = \frac{1}{n_r} \sum_{i=1}^{n_r} (\mathcal{N}[f_\theta(\mathbf{x}_i^r)] - g(\mathbf{x}_i^r))^2, \quad (5)$$

where $\{\mathbf{x}_i^r\}_{i=1}^{n_r} \subset \Omega$ are collocation points, and $\mathcal{N}[f_\theta(x)]$ is computed accurately using automatic differentiation methods [30]. The neural network is fitted to the initial and boundary condition $h(x)$ using a traditional data-fitting loss function:

$$\mathcal{L}_b = \frac{1}{n_b} \sum_{i=1}^{n_b} |f_\theta(\mathbf{x}_i^b) - h(\mathbf{x}_i^b)|^2 \quad (6)$$

where $\{\mathbf{x}_i^b\}_{i=1}^{n_b} \subset \partial\Omega$ are initial and boundary points. If there are experimental or simulation data $\{\mathbf{x}_i^d, \mathbf{y}_i^d\}_{i=1}^{n_d}$ available, they may be include into a data loss:

$$\mathcal{L}_d = \frac{1}{n_d} \sum_{i=1}^{n_d} |f_\theta(\mathbf{x}_i^d) - \mathbf{y}_i^d|^2. \quad (7)$$

The previous multi-objective optimization problem is typically solved by simple linear scalarization, in which case the PINN is trained by minimizing the total loss function \mathcal{L} :

$$\mathcal{L} = \mathcal{L}_r + \mathcal{L}_b + \mathcal{L}_d. \quad (8)$$

This framework is also easily extended to more complex initial and boundary conditions.

2.3 Particle Swarm Optimization

The Particle Swarm Optimization (PSO) algorithm [31, 32] is a population-based stochastic optimization algorithm that emulates the swarm behavior of particles distributed in a n -dimensional search space [33]. Each individual in this swarm represents a candidate solution. At each iteration, the particles in the swarm exchange information and use it to update their positions. Particle $\theta(t)$ at iteration t is guided by a velocity determined by three factors: its own velocity inertia $\beta V(t)$, its best-known position p_{best} in the search-space, as well as the entire swarm's best-known position g_{best} :

$$V(t+1) = \beta V(t) + c_1 r_1 (p_{best} - \theta(t)) + c_2 r_2 (g_{best} - \theta(t)), \quad (9)$$

where c_1 and c_2 are the cognitive and social coefficients, respectively, and r_1 and r_2 are uniformly distributed random numbers in range $[0, 1)$. Then the particle position is updated as

$$\theta(t+1) = \theta(t) + V(t+1). \quad (10)$$

Many variations of the PSO algorithm were proposed over time, including a hybrid PSO and gradient-based algorithm known as PSO-BP[34], which adds a gradient descent component to the swarm framework. This strategy came particularly handy when applying the method to train neural networks since all partial gradients can be computed efficiently by backpropagation. In the PSO-BP algorithm, the particle's velocity is updated via (contrast this to equation 9):

$$\begin{aligned} V(t+1) = & \beta V(t) + c_1 r_1 (p_{best} - \theta(t)) \\ & + c_2 r_2 (g_{best} - \theta(t)) - \alpha \nabla \mathcal{L}(\theta(t)), \end{aligned} \quad (11)$$

where α is the learning rate and $\nabla \mathcal{L}(\theta(t))$ is the loss gradient. Therefore, the gradient participates in the velocity magnitude and direction, by an amount that is specified by the learning rate.

3 PSO-PINN Algorithm

The objective of this work is a new approach to train a PINN, which avoids using pure gradient descent backpropagation by using "swarms" (ensembles) of PINNs. In this section, we present three different models, how to initialize them, and a few possible ways to summarize the ensemble results.

3.1 The Models

The three alternatives for the model are listed below. The first is the original PSO algorithm (as described in equations 9 and 10), the second is an adaptation of the PSO-BP (adding a gradient component to the algorithm, as described in equation 11), and the third one is PSO-BP with parameters updates.

1. **Original PSO** - The PSO in its original form. Each particle on the Swarm would be a candidate solution, i.e. a neural network.
2. **PSO-BP** - In addition to the population components, this version has a component based on the derivative gradient of the loss function. Equation 11 displays the changes made in this version.
3. **PSO-BP + parameters updates** The behavioral components c_1 and c_2 decay linearly with iteration number as follows:

$$c_k^i = c_k^i - \frac{2c_k^i}{n} \quad (12)$$

for $k = 1, 2$ and $i = 1, 2, \dots, n$, where n is the total number of iterations.

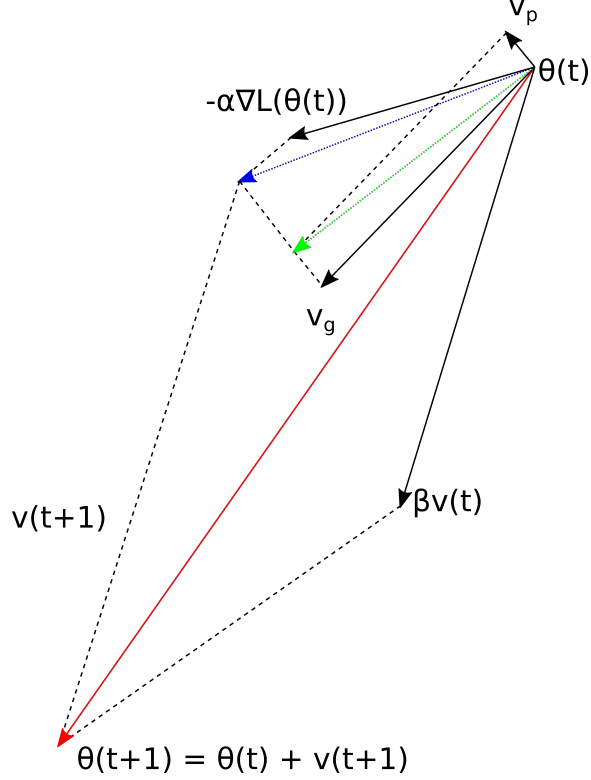


Figure 1: **PSO-PINN update** – The green vector is the PSO resultant (from the cognitive and social movements). The blue arrow is the resultant after adding the gradient movement ($-\alpha \nabla \mathcal{L}(\theta(t))$) vector. Finally, the red vector represents the total movement, after including the particle inertia.

3.2 The Algorithm

The PSO-PINN swarm is an ensemble of potential PINN candidates. Each particle in the swarm is a vector θ containing the weights and biases of the corresponding PINN. Let Θ denote the population of all particles. The ensemble of PINNs is updated according to Algorithm 1.

Let Θ be randomly initialized as a set of θ (following one of the methods listed in section 4.3), as described in Equation 1. Also, define the objective function $f(\theta)$ as a scalar function that is differentiable w.r.t. parameters θ . In the specific case of PINNs, we may use the loss function as described in Equation 8. The p_{best} vector should be initialized with the Θ population, as the particles know nothing but their initial point at this time. The g_{best} parameter should assume the value of θ for the minimum $f(\theta)$ (constrained to $\theta \in \Theta$). In practice, the gradient descent component is not implemented by a simple gradient step $\alpha \nabla \mathcal{L}(\theta(t))$, but rather by ADAM optimization [6].

After the initialization setup, the updates to the swarm attempt to minimize the expected value of the objective function $\mathbb{E}[f(\theta)]$. The particle velocities and locations are updated at each iteration following equations 9 and 10, respectively. After that, the new value $f(\Theta_{i+1})$ is compared with the old value $f(\Theta_i)$. The value of p_{best} will be the set of θ where $f(\Theta_{i+1}) < f(\Theta_i)$, whereas g_{best} will adopt the best value θ for which $f(\Theta)$ attains its minimum. Figure 1 illustrates the movement forces acting at each iteration. The loop runs either until Θ converges, or a maximum number of iterations is reached.

3.3 Ensembles

Beyond the fact that swarms are a well-established optimization method, they also provide an ensemble of solutions. Thus, we can take advantage of the various properties provided by ensembles. This category of learning methods combines individual models to create a ‘‘consensus’’ model, which is expected to display improved performance and stability than any of the individual models. There are several different methods to find the consensus decision from an ensemble [13]. The most straightforward one perhaps would simply

Algorithm 1: PSO-PINN

Require: α : Step-size;
Require: β : Inertia;
Require: c_1, c_2 : cognitive and social coefficients;
Require: $\mathcal{L}(\theta)$: Loss for PINN with parameters θ ;
 Initialize Population Θ ;
 $p_{best} \leftarrow \Theta$;
 $g_{best} \leftarrow \arg \min_{\theta} (p_{best})$;
for $t = \{0, 1, 2, \dots\}$ **do**:
 for $\theta \in \Theta$ **do**:
 $r_1, r_2 \leftarrow U(0, 1]$;
 $V(t+1) = \beta V(t) +$
 $c_1 r_1 (p_{best} - \theta(t)) +$
 $c_2 r_2 (g_{best} - \theta(t)) -$
 $\alpha \nabla \mathcal{L}(\theta(t))$;
 $\theta(t+1) = \theta(t) + V(t+1)$;
 $p_{best} \leftarrow \{\theta(t+1), \text{if } \mathcal{L}(\theta(t+1)) < \mathcal{L}(p_{best})$
 $p_{best}, \text{otw}\}$;
end
 $g_{best} \leftarrow \operatorname{argmin}_{\theta} (p_{best})$;
if parameter_updates:
 $c_1 = c_1 - \frac{2c_1}{t}$
 $c_2 = c_2 - \frac{c_2}{t}$
if converged **break**;
end

choose the best-fitted model according to the loss function. Although this may yield a good model, it could fail due to overfitting. To avoid this, a better approach exploits the ensemble diversity through model averaging:

$$\hat{f}_{\theta}(x) = \frac{1}{|\Theta|} \sum_{\theta_i \in \Theta} f_{\theta_i}(x). \quad (13)$$

This approach also leads naturally to uncertainty quantification, as the covariance matrix can be considered as a measure of the uncertainty of the ensemble:

$$\Sigma_{f_{\theta}(x)} = \frac{1}{|\Theta| - 1} \sum_{\theta_i \in \Theta} (f_{\theta_i}(x) - \hat{f}_{\theta}(x))(f_{\theta_i}(x) - \hat{f}_{\theta}(x))^{\top} \quad (14)$$

4 Experiments and Results

In this section, we present experimental results that demonstrate the performance of PSO-PINN using several classical ODE and PDE benchmarks. After presenting the solutions of the various equations obtained by PSO-PINN, we discuss possible parametrizations for the algorithm, and finally we compare the PSO-PINN to a pure ensemble of ADAM-trained PINNs, without communication among the PINNs as in PSO-PINN. The main figure of merit used in this section is the L_2 error:

$$L_2 \text{ error} = \frac{\sqrt{\sum_{i=1}^{N_U} |\hat{f}_{\theta}(x_i) - U(x_i)|^2}}{\sqrt{\sum_{i=1}^{N_U} |U(x_i)|^2}}. \quad (15)$$

where $\hat{f}_{\theta}(x)$ is the prediction and $U(x)$ is the analytical solution or a high-fidelity approximation over a mesh $\{x_i\}$ containing N_U points. All experiments in this section were performed using Tensorflow 2.x[35].

4.1 Benchmarks

We describe below several PDE and ODE benchmarks and display the solutions obtained by PSO-PINN.

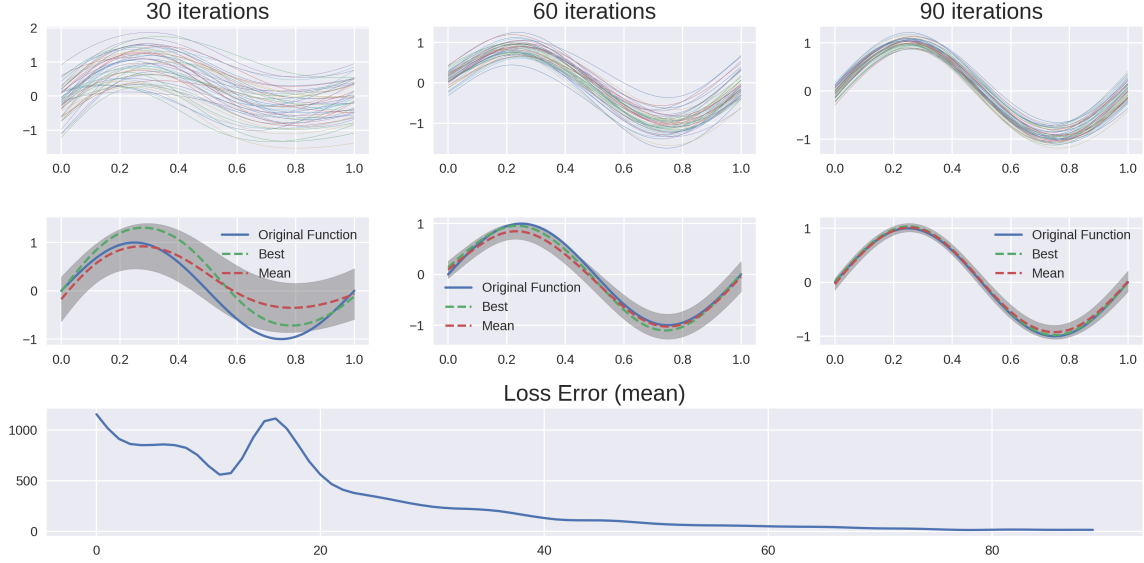


Figure 2: **Poisson Equation** – First row: solutions in the PSO-PINN ensemble as training progresses. Second row: Best individual, mean and variance of PSO-PINN ensemble. Third row: PSO-PINN mean loss error.

4.1.1 Poisson Equation

The first problem is the 1D Poisson equation, which is an ordinary differential equation defined by:

$$\begin{aligned} u_{xx} &= g(x), \quad x \in [0, 1], \\ u(0) &= a, \\ u(1) &= b. \end{aligned} \quad (16)$$

For this example, we manufacture $g(x)$ so that $u(x) = \sin(2\pi x)$, with $u(0) = u(1) = 0$. Since this problem describes an ODE (relatively simpler than a PDE), we may use a relatively shallow architecture. In this case, we are using a network with 3 layers of 10 neurons, trained for only 90 iterations. The particles in the PSO-PINN swarm were initialized using the uniform distribution and the values assigned for β , c_1 and c_2 were 0.9, 0.08, and 0.5, respectively.

Figure 2 displays the results. We can see that the PSO-PINN swarm finds an excellent approximation to the solution rather quickly, in less than one hundred iterations. Also, the mean and variance show that the entire swarm has good convergence. The variance of the swarm may be interpreted as the uncertainty associated with the approximation. As the swarm approach a consensus we should notice a reduction in the variance of the solution, indicating more confidence in the final result.

4.1.2 The Advection Equation

The advection equation models the transport of a substance by bulk motion of a fluid. In this example, we are assuming a linear univariate advection equation [36]:

$$q_t + uq_x = 0 \quad (17)$$

where u is the constant velocity. The Riemman initial condition is

$$q(x, 0) = \begin{cases} q_l, & 0 \leq x < x_0, \\ q_r, & x_0 < x \leq L. \end{cases} \quad (18)$$

This simple problem has as solution:

$$q(x, t) = \begin{cases} q_l, & 0 \leq x < x_0 + ut, \\ q_r, & x_0 + ut < x \leq L, \end{cases} \quad (19)$$

for $0 \leq t < (L - x_0)/u$. In other words, the initial discontinuity in concentration is simply advected to the left with constant speed u .

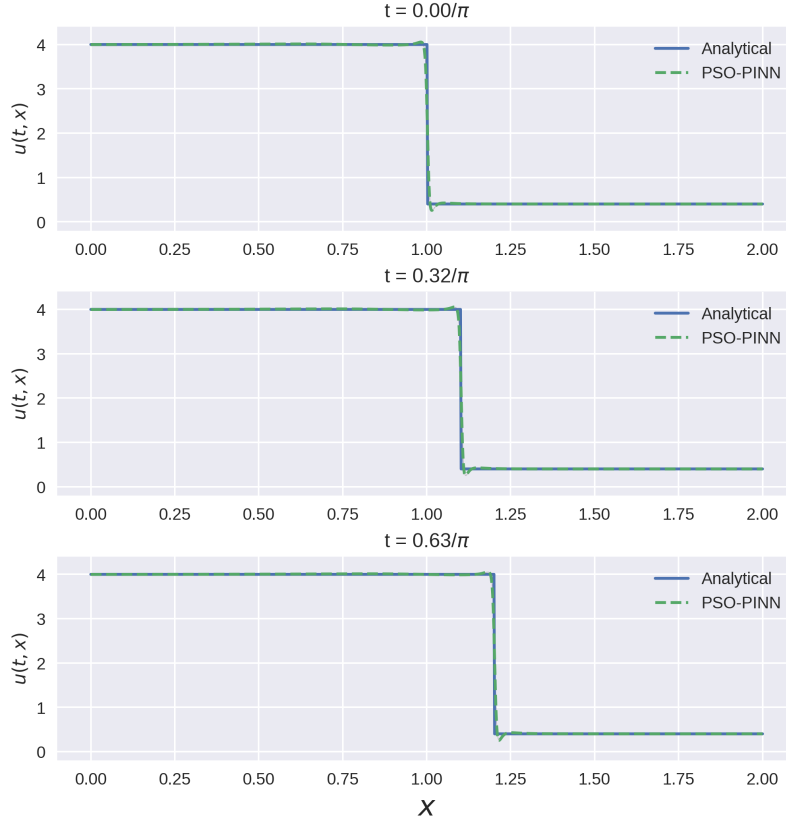


Figure 3: **Advection Equation** – The PSO-PINN solution is the mean values of the results in the swarm.

For this problem we used a PSO-PINN swarm composed of 50 particles, each one with 5 layers of 8 neurons, and trained it through 500 iterations. The PSO attributes β , c_1 , and c_2 were set to 0.99, 0.008 and 0.05, respectively. Figure 3 shows that PSO-PINN found a good approximation after just 500 iterations. There was good convergence to the true solution, with L_2 error for the depicted result equal to $4.71\text{E-}2$ and mean variance equal to $1.38\text{E-}2$.

4.1.3 Burgers Equation

Here we consider the following version of the the viscous Burgers equation:

$$\begin{aligned} \frac{\partial u}{\partial t} + u \frac{\partial u}{\partial x} &= \nu \frac{\partial^2 u}{\partial x^2}, & x \in [-1, 1], \quad t \in [0, 1] \\ u(0, x) &= -\sin(\pi x), \\ u(t, -1) &= u(t, 1) = 0, \end{aligned} \tag{20}$$

with $\nu = 0.01/\pi$

For the Burgers equation we trained a PSO-PINN with 8 hidden layers of 10 neurons each, and an output layer of size 1 corresponding to the output of the approximation $u(x, t)$. We used a swarm containing 20 particles (networks), and the algorithm was trained for 2000 iterations with the values of β , c_1 , and c_2 to 0.9, 0.04 and 0.05, respectively. After 10 consecutive experiments, the median for the L_2 error was $1.25\text{E-}2$ and for the best ensemble the L_2 error was $5.79\text{E-}2$. More details can be seen on the Table 1.

4.1.4 The Heat Equation

We solve a 1D Heat equation, which models the temperature dissipation in an iron rod.

$$\begin{aligned} \frac{\partial u}{\partial t} &= \alpha \frac{\partial^2 u}{\partial x^2}, & x \in [-1, 1], & \quad t \in [0, 1] \\ u(0, t) &= u(1, t) = 0, \\ u(x, 0) &= \sin\left(\frac{n\pi x}{L}\right), & 0 < x < L \end{aligned} \quad (21)$$

where $L = 1$ is the length of the bar, $n = 1$ is the frequency of the sinusoidal initial conditions. The reference solution is $u(x, t) = e^{-\frac{n^2\pi^2\alpha t}{L^2}} \sin(\frac{n\pi x}{L})$. The results displayed in Figure 4 represents a PSO-PINN solution of a network with 8 layers of 20 neurons each. The swarm was composed by 20 particles and it ran over 4000 iterations. The experiment resulted in a L_2 error obtained was 8.18E-3.

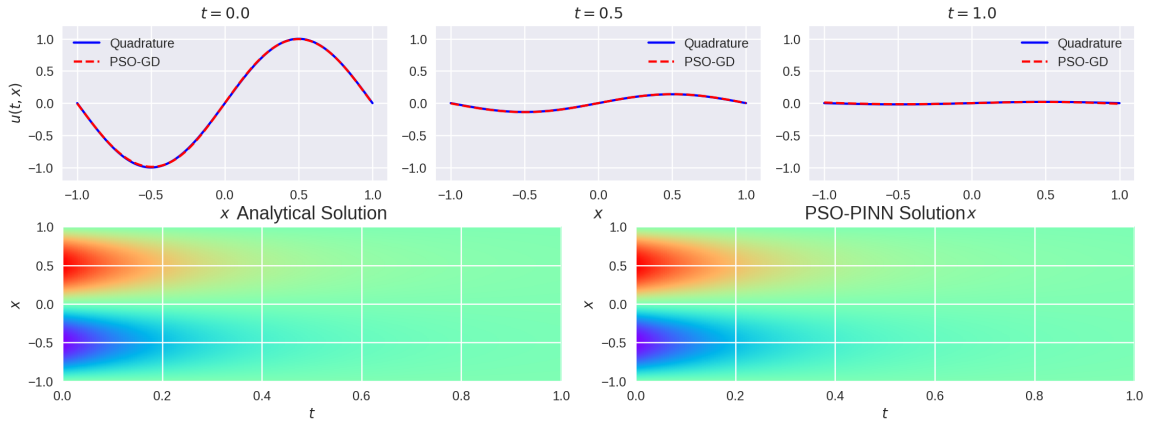


Figure 4: **Heat Equation** – In the first row is the cross-section PSO-PINN solution for the problem (the mean values of the swarm predictions). The second row shows the results for the entire domain. The last row displays the analytical solution.

4.1.5 The Diffusion Equation

This example also describes a 1D heat diffusion equation. We are calling this benchmark the diffusion equation for the sake of organization. The PDE is given by:

$$\begin{aligned} \frac{\partial u}{\partial t} - \frac{\partial^2 u}{\partial x^2} &= 1 + x \cos(t) & x \in [-1, 1], & \quad t \in [0, 1] \\ \frac{\partial u}{\partial x} \Big|_{x=0} &= \frac{\partial u}{\partial x} \Big|_{x=1} = \sin(t), \\ u(x, 0) &= 1 + \cos(2\pi x) \end{aligned} \quad (22)$$

The exact solution is $u(x, t) = 1 + t + e^{-4\pi^2 t} \cos(2\pi x) + x \sin(t)$.

For this example we trained a PSO-PINN with 20 particles. Each element is a network with 5 layers of 8 neurons and they were trained for 2000 iterations. The values of β , c_1 , and c_2 to 0.99, 0.008 and 0.05, respectively. After 10 consecutive experiments, the median for the L_2 error was 3.23E-2. More details on the Table 1.

4.1.6 The Allen-Cahn Equation

The Allen-Cahn reaction-diffusion PDE is typically used to describe phase-field models to simulate the phase separation in a multi-component alloy. The Allen-Cahn equation is described as follows:

$$\begin{aligned}
 \frac{\partial u}{\partial t} &= d \frac{\partial^2 u}{\partial x^2} + 5(u - u^3), \quad x \in [-1, 1], \quad t \in [0, 1] \\
 u(x, 0) &= x^2 \cos(\pi x) \\
 u(-1, t) &= u(1, t) = -1
 \end{aligned} \tag{23}$$

For the simulations on this paper we kept $d = 0.0001$. We used a PSO-PINN swarm of 20 particles, each one representing a neural network with 5 hidden layers and 20 neurons per layer. In this particular example, we added data points in the domain to aid training (this benchmark is notoriously hard for PINNs to solve [9]). The dataset is composed of ten evenly spaced points in the x axis extended over the t domain at 200 intervals.

4.2 Model Selection

Most meta-heuristics algorithms for optimization, especially in the PSO family, are rather sensitive to their control parameters[37, 38]. This peculiarity may turn the parametrization of the algorithm into a challenging task. For this reason, we performed reiterative experiments, using rounds of 10 repetitions for each parametrization, collected and analyzed the results to better understand each parameter’s share of the outcome from the PINN.

We use the four PDE problems described in the last section as a baseline to analyse the models, initializations, and ensembles generated by the swarms (except for the Allen-Cahn equation, since we are using data in this benchmark). We did a grid search over the parameters (α , β , c_1 , and c_2) and initializations of the PSO-PINN algorithm aiming to find the best parametrization for each pair problem/model. The hyper-parameters were kept fixed over all experiments, in order to give a better perspective on the outcomes of the PSO-PINN, especially after changes on the models and initializations. The population of the ensembles was kept fixed at 20 individuals, where each individual was a PINN with 5 layers and 8 neurons per layer trained for 2000 iterations.

The Table 1 shows the summary of this experiments. We listed the results for each problem described before, using each one of models presented in section 3.1. The columns α , β , c_1 , and c_2 , on its turn, represent the best parameters for each problem/model. Finally, the last four columns exhibit the results for the given experiment. The mean, median and variance are the average values after the 10 rounds of tests and the best column give us the best particle from the best swarm.

As shown in the table, the gradient-assisted optimization achieved the best results for all the proposed problems, either using parameters updating(model 3) or not (model 2). Also, we had a consensus for the best value for the α (Adam’s learning rate) as 0.001. Despite the values for β , c_1 and c_2 were not unanimous among the results, good results are often obtained using 0.9, 0.04 and 0.5, respectively.

4.3 Initialization

The initialization of the weights of a Neural Network may have a critical impact on the training process, which often reflects on model performance. One of the most accepted methods for initialization is the Xavier Initialization[39], which attempts to keep the same variance across every layer. However, although this approach has been vastly used to initialize deep neural networks, it only takes into account a single neural network.

It is yet to be proven that such initialization could yield a better population for an ensemble of neural nets (especially for a swarm, the current literature suggests to have an evenly dispersed over the search space). During the initialization of a swarm, we want to cover the search space as much as possible[40], and there is no evidence that such method could expand the search space concerning the whole swarm. This subject was discussed to some extent in [41].

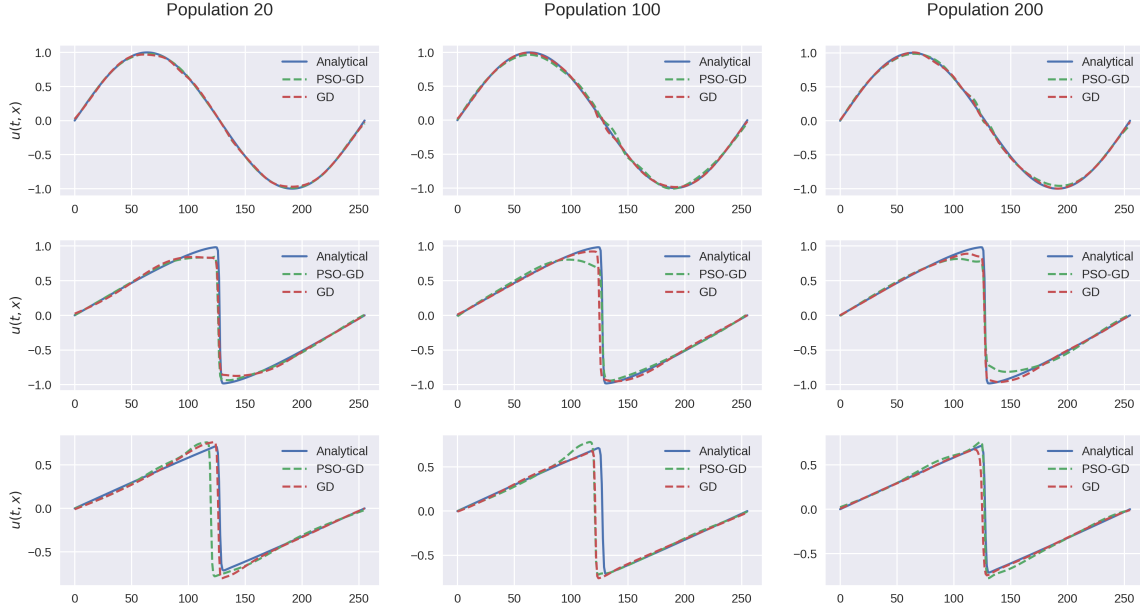
We did a brief investigation on how different network initialization would affect the swarm behavior. In Table 1, we can notice that different problems alongside with different parametrizations required distinct initialization methods. Interestingly, uniform initialization seemed to work well for the Advection and the Diffusion problems. The table 2 summarises the results obtained grouping all the parametrizations used for each initialization. Notice that changes in the initialization are much less sensitive than changes on the parametrization. This leads us to infer that even if the initialization method must have some level of influence on the final predictor, it is smaller than the changes in the parameters, but it is still noticeable in the final predictor. As well as in the case of parametrizations, the ideal initialization may vary depending on the problem and the parameters. However, the uniform initialization showed a consistent performance in all experiments.

Table 1: **Model Selection** – The following configurations are the result of a grid search over the initializations, α , β , c_1 , c_2 for each model.

Problem	Model	Optimizer	Initialization	α	β	c_1	c_2	L_2 Error			
								Mean	Median	Variance	Min
Advection	1	PSO	uniform	-	0.99	0.08	0.05	7.08E-02	6.44E-02	2.47E-03	2.25E-02
	2	PSO-PINN	uniform	0.001	0.9	0.04	0.5	3.51E-02	3.46E-02	1.24E-05	3.02E-02
	3	PSO-PINN	uniform	0.001	0.99	0.008	0.05	3.27E-02	3.29E-02	4.35E-06	2.84E-02
Burgers	1	PSO	he	-	0.99	0.08	0.05	4.54E-01	4.57E-01	4.59E-03	3.22E-01
	2	PSO-PINN	he	0.001	0.9	0.04	0.05	1.47E-01	1.25E-01	5.37E-03	5.79E-02
	3	PSO-PINN	he	0.001	0.99	0.08	0.5	1.78E-01	1.51E-01	5.75E-03	8.73E-02
Diffusion	1	PSO	uniform	-	0.99	0.008	0.05	4.95E-02	4.92E-02	3.78E-06	4.77E-02
	2	PSO-PINN	uniform	0.001	0.9	0.04	0.5	1.99E-02	1.29E-02	2.28E-04	7.15E-03
	3	PSO-PINN	uniform	0.001	0.9	0.08	0.05	2.17E-02	1.40E-02	2.35E-04	1.09E-02
Heat	1	PSO	xavier	-	0.99	0.008	0.05	2.62E-01	2.47E-01	2.07E-03	1.91E-01
	2	PSO-PINN	he	0.001	0.9	0.04	0.5	6.60E-03	5.57E-03	7.61E-06	3.68E-03
	3	PSO-PINN	lecun	0.001	0.9	0.008	0.5	5.14E-03	5.26E-03	2.88E-06	2.13E-03

Table 2: **Initialization Methods** – The median of the L_2 errors of the predictors for each problem according to the initialization method.

Initialization	Advection	Burgers	Diffusion	Heat
He	4.46E-02	3.02E-01	4.66E-02	1.41E-02
Lecun	4.44E-02	3.74E-01	4.91E-02	1.02E-02
Uniform	4.05E-02	3.19E-01	4.70E-02	1.84E-02
Xavier	4.81E-02	3.24E-01	4.99E-02	2.37E-02


 Figure 5: **Burger Equation** – PSO-PINN produce the best results. The results for the baseline PINN with gradient descent were repeated across the columns for comparison purposes.

4.4 Comparison with Traditional Ensembles of PINNs

In this section we investigate the performance of the PSO-PINN algorithm in three different problems, comparing it to ensembles of Adam-trained PINNs. In this comparison, to keep the comparison fair, both methods shared the same network topology (5 hidden layers of 8 neurons), number of iterations (2000), number of collocation points (512) and same size of population (20 particles).

4.4.1 Burgers Equation

Figure 5 illustrates the effect of population size on the accuracy of PSO-PINN. The first column represents the solution using a population of twenty particles, the second and third columns show the solution for a hundred and two hundreds, respectively. In all the cases the ensembles were trained for 2000 iterations. Clearly, the results improve with a larger number of particles, especially for PSO-PINN. This is the expected behavior, since we are in fact increasing the exploration of the search space.

4.4.2 Diffusion Equation

The Figure 6 shows the solution for the Diffusion equation as described in equation 22. The figure depicts the spatial-temporal domain, where the x -axis represents the time(t) and the y -axis represents the space(x). In the first row we have the analytical high-fidelity solution, the second and third rows illustrate the solutions given by the PSO-PINN and the Adam ensemble, respectively. Notably, the PSO-PINN obtained a better approximation to the original PDE, especially in the first half of the time dimension. The L_2 error PSO-PINN found in the PSO-PINN solution was 6.54E-02, while the error for the Adam ensemble was 1.05E-01.

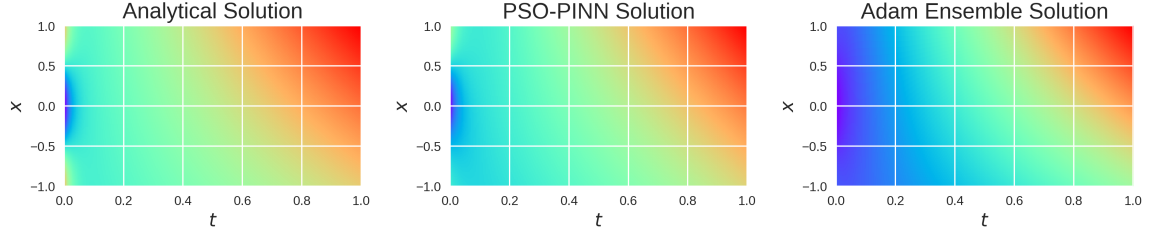


Figure 6: **Diffusion Equation** – Results across the spatial-temporal domain. The first row represents the high-fidelity analytical solution. In the second row is the PSO-PINN solution, and in the third row the solution from an ensemble of traditional PINNs using ADAM as optimizer.

4.4.3 Allen-Cahn Equation

The Allen-Cahn Equation (described in equation 23) is used here to illustrate the usage of supplementary data to solve a PDE. We previously created a dataset distributed over the domain $x \in [-1, 1]$, and $t \in [0, 1]$ and use it to give supplementary information for solving the problem. The purpose is to show that PSO-PINN framework incorporates well the data Loss (\mathcal{L}_d). The solutions for the problem are represented in Figure 7. We can see that both ensembles had good results, although the PSO-PINN reached general better precision. When compared with an ensemble of traditional PINNs using Adam optimization, we can notice that the PSO-PINN algorithm was able to reduce uncertainty in certain locations of the spatial-temporal domain.

These experiments display promising results for PINN training using swarm intelligence and ensemble models. It was seen that PSO-PINN consistently outperformed the baseline PINN trained with Adam gradient descent.

Additionally, PSO-PINN provides the advantages of an ensemble approach. In this paper, we used the mean/best and variance of the PSO-PINN ensemble as a predictor and its corresponding uncertainty, respectively. However, other ensemble techniques, such as stacking [42] and snapshot [43], could be used with PSO-PINN and bring practical benefits in increased accuracy, better uncertainty quantification, and more robust predictions.

We observed that better performance is associated with a larger ensemble size. Although this means a larger computational cost, this could be mitigated by using parallelization. There are out-of-the-shelf implementations in TensorFlow to parallelize tensors calculations, and PSO-PINN is already taking advantage of that. Nevertheless, there is room for improvement, mainly regarding distributed training strategies. Such procedures would allow PSO-PINN to distribute its training across multiple GPUs, clusters, multiple machines, or even Cloud TPUs.

5 Conclusion

This paper proposed PSO-PINN, a particle-swarm optimization methodology for training physics-informed neural networks. PSO-PINN is based on PSO-BP, a previously proposed hybrid particle swarm optimization-gradient descent algorithm for training deep neural networks. PSO-PINN produces an ensemble of PINN solutions, which allows variance estimation for quantifying the uncertainty in the prediction. A more considerable degree of agreement among the PINNs leads to small variance and a higher degree of confidence in the predicted values. Other ensemble techniques, such as stacking [42] and snapshot [43], can be readily introduced into the PSO-PINN framework to produce even better predictions and uncertainty quantification.

The PSO-PINN ensembles are usually more robust than ensembles composed by PINNs trained independently (using Adam optimization). They are more precise and often has less variance, leading to a greater confidence in the solution proposed.

However, the proposed model is sensitive to parameter setting. Most of the parameters require fine-tuning to perform well, and occasionally some parametrizations yield unstable predictors with high variance over particles and swarms. In some severe cases, even random seed changes could drastically modify the results.

Some other aspects of swarm optimization are yet to be explored, such as multi-objective optimization, which would be quite suitable for PINNs, since its total loss function is nothing more than a scalarization of multiple

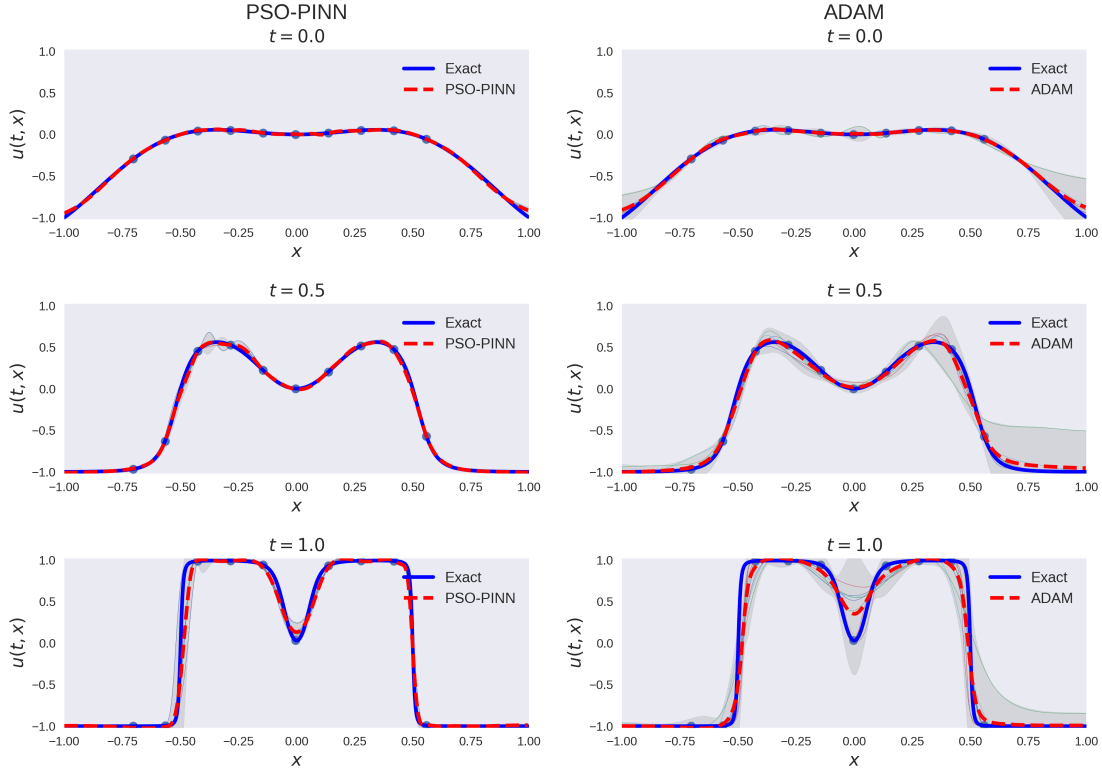


Figure 7: **Allen-Cahn Equation** –The result depicted as cross-sections above the spatial-temporal domain. The left column show the PSO-PINN solution and the right column show the solution for an ensemble of traditional PINNs optimized using Adam.

losses (often minimized as the sum of the losses). Also, distributing computing strategies might unleash several possibilities, enabling high scalability and new approaches for optimization.

Future work will explore these and other improvements in the PSO-PINN methodology in order to tackle more challenging problems, including inverse mapping of equation parameters and unobserved variables in high-dimensional problems.

References

- [1] M. Raissi, P. Perdikaris, and G. E. Karniadakis, “Physics-informed neural networks: A deep learning framework for solving forward and inverse problems involving nonlinear partial differential equations,” *Journal of Computational Physics*, vol. 378, pp. 686–707, 2019.
- [2] M. Raissi, A. Yazdani, and G. E. Karniadakis, “Hidden fluid mechanics: Learning velocity and pressure fields from flow visualizations,” *Science*, vol. 367, no. 6481, pp. 1026–1030, 2020.
- [3] G. E. Karniadakis, I. G. Kevrekidis, L. Lu, P. Perdikaris, S. Wang, and L. Yang, “Physics-informed machine learning,” *Nature Reviews Physics*, vol. 3, no. 6, pp. 422–440, 2021.
- [4] K. Hornik, M. Stinchcombe, and H. White, “Multilayer feedforward networks are universal approximators,” *Neural networks*, vol. 2, no. 5, pp. 359–366, 1989.
- [5] S.-i. Amari, “Backpropagation and stochastic gradient descent method,” *Neurocomputing*, vol. 5, no. 4-5, pp. 185–196, 1993.
- [6] D. P. Kingma and J. Ba, “Adam: A method for stochastic optimization,” *arXiv preprint arXiv:1412.6980*, 2014.

- [7] S. Wang, Y. Teng, and P. Perdikaris, “Understanding and mitigating gradient flow pathologies in physics-informed neural networks,” *SIAM Journal on Scientific Computing*, vol. 43, no. 5, pp. A3055–A3081, 2021.
- [8] S. Wang, X. Yu, and P. Perdikaris, “When and why pinns fail to train: A neural tangent kernel perspective,” *Journal of Computational Physics*, vol. 449, p. 110768, 2022.
- [9] L. McClenny and U. Braga-Neto, “Self-adaptive physics-informed neural networks using a soft attention mechanism,” *arXiv preprint arXiv:2009.04544*, 2020.
- [10] R. van der Meer, C. W. Oosterlee, and A. Borovykh, “Optimally weighted loss functions for solving pdes with neural networks,” *Journal of Computational and Applied Mathematics*, p. 113887, 2021.
- [11] A. D. Jagtap and G. E. Karniadakis, “Extended physics-informed neural networks (xpinns): A generalized space-time domain decomposition based deep learning framework for nonlinear partial differential equations,” *Communications in Computational Physics*, vol. 28, no. 5, pp. 2002–2041, 2020.
- [12] K. Shukla, A. D. Jagtap, and G. E. Karniadakis, “Parallel physics-informed neural networks via domain decomposition,” *arXiv preprint arXiv:2104.10013*, 2021.
- [13] M. Ganaie, M. Hu, *et al.*, “Ensemble deep learning: A review,” *arXiv preprint arXiv:2104.02395*, 2021.
- [14] L. K. Hansen and P. Salamon, “Neural network ensembles,” *IEEE transactions on pattern analysis and machine intelligence*, vol. 12, no. 10, pp. 993–1001, 1990.
- [15] Y. Cao, T. A. Geddes, J. Y. H. Yang, and P. Yang, “Ensemble deep learning in bioinformatics,” *Nature Machine Intelligence*, vol. 2, no. 9, pp. 500–508, 2020.
- [16] L. Deng and J. Platt, “Ensemble deep learning for speech recognition,” in *Proc. interspeech*, 2014.
- [17] X. Qiu, L. Zhang, Y. Ren, P. N. Suganthan, and G. Amaratunga, “Ensemble deep learning for regression and time series forecasting,” in *2014 IEEE symposium on computational intelligence in ensemble learning (CIEL)*, pp. 1–6, IEEE, 2014.
- [18] K. Haitsiukevich and A. Ilin, “Improved training of physics-informed neural networks with model ensembles,” *arXiv preprint arXiv:2204.05108*, 2022.
- [19] J. Kennedy and R. Eberhart, “Particle swarm optimization,” in *Proceedings of ICNN’95-international conference on neural networks*, vol. 4, pp. 1942–1948, IEEE, 1995.
- [20] A. Chakraborty and A. K. Kar, “Swarm intelligence: A review of algorithms,” *Nature-Inspired Computing and Optimization*, pp. 475–494, 2017.
- [21] F. Van den Bergh and A. P. Engelbrecht, “Cooperative learning in neural networks using particle swarm optimizers,” *South African Computer Journal*, vol. 2000, no. 26, pp. 84–90, 2000.
- [22] G. Das, P. K. Pattnaik, and S. K. Padhy, “Artificial neural network trained by particle swarm optimization for non-linear channel equalization,” *Expert Systems with Applications*, vol. 41, no. 7, pp. 3491–3496, 2014.
- [23] S. Mirjalili, “How effective is the grey wolf optimizer in training multi-layer perceptrons,” *Applied Intelligence*, vol. 43, no. 1, pp. 150–161, 2015.
- [24] S. J. Mousavirad, G. Schaefer, S. M. J. Jalali, and I. Korovin, “A benchmark of recent population-based metaheuristic algorithms for multi-layer neural network training,” in *Proceedings of the 2020 genetic and evolutionary computation conference companion*, pp. 1402–1408, 2020.
- [25] B. Lakshminarayanan, A. Pritzel, and C. Blundell, “Simple and scalable predictive uncertainty estimation using deep ensembles,” *arXiv preprint arXiv:1612.01474*, 2016.
- [26] A. Krizhevsky, I. Sutskever, and G. E. Hinton, “Imagenet classification with deep convolutional neural networks,” *Advances in neural information processing systems*, vol. 25, pp. 1097–1105, 2012.
- [27] R. K. Yadav *et al.*, “Pso-ga based hybrid with adam optimization for ann training with application in medical diagnosis,” *Cognitive Systems Research*, vol. 64, pp. 191–199, 2020.
- [28] Y. LeCun, Y. Bengio, and G. Hinton, “Deep learning,” *nature*, vol. 521, no. 7553, pp. 436–444, 2015.
- [29] X. Glorot, A. Bordes, and Y. Bengio, “Deep sparse rectifier neural networks,” in *Proceedings of the fourteenth international conference on artificial intelligence and statistics*, pp. 315–323, JMLR Workshop and Conference Proceedings, 2011.
- [30] A. G. Baydin, B. A. Pearlmutter, A. A. Radul, and J. M. Siskind, “Automatic differentiation in machine learning: a survey,” *Journal of machine learning research*, vol. 18, 2018.

- [31] R. Eberhart and J. Kennedy, "Particle swarm optimization," in *Proceedings of the IEEE international conference on neural networks*, vol. 4, pp. 1942–1948, Citeseer, 1995.
- [32] Y. Shi and R. C. Eberhart, "Empirical study of particle swarm optimization," in *Proceedings of the 1999 congress on evolutionary computation-CEC99 (Cat. No. 99TH8406)*, vol. 3, pp. 1945–1950, IEEE, 1999.
- [33] D. Wang, D. Tan, and L. Liu, "Particle swarm optimization algorithm: an overview," *Soft Computing*, vol. 22, no. 2, pp. 387–408, 2018.
- [34] R. K. Yadav *et al.*, "Ga and pso hybrid algorithm for ann training with application in medical diagnosis," in *2019 Third International Conference on Intelligent Computing in Data Sciences (ICDS)*, pp. 1–5, IEEE, 2019.
- [35] M. Abadi, A. Agarwal, P. Barham, E. Brevdo, Z. Chen, C. Citro, G. S. Corrado, A. Davis, J. Dean, M. Devin, S. Ghemawat, I. Goodfellow, A. Harp, G. Irving, M. Isard, Y. Jia, R. Jozefowicz, L. Kaiser, M. Kudlur, J. Levenberg, D. Mané, R. Monga, S. Moore, D. Murray, C. Olah, M. Schuster, J. Shlens, B. Steiner, I. Sutskever, K. Talwar, P. Tucker, V. Vanhoucke, V. Vasudevan, F. Viégas, O. Vinyals, P. Warden, M. Wattenberg, M. Wicke, Y. Yu, and X. Zheng, "TensorFlow: Large-scale machine learning on heterogeneous systems," 2015. Software available from tensorflow.org.
- [36] R. J. LeVeque *et al.*, *Finite volume methods for hyperbolic problems*, vol. 31. Cambridge university press, 2002.
- [37] B. J. Leonard and A. P. Engelbrecht, "On the optimality of particle swarm parameters in dynamic environments," in *2013 IEEE congress on evolutionary computation*, pp. 1564–1569, IEEE, 2013.
- [38] K. R. Harrison, A. P. Engelbrecht, and B. M. Ombuki-Berman, "Self-adaptive particle swarm optimization: a review and analysis of convergence," *Swarm Intelligence*, vol. 12, no. 3, pp. 187–226, 2018.
- [39] X. Glorot and Y. Bengio, "Understanding the difficulty of training deep feedforward neural networks," in *Proceedings of the thirteenth international conference on artificial intelligence and statistics*, pp. 249–256, JMLR Workshop and Conference Proceedings, 2010.
- [40] P. Cazzaniga, M. S. Nobile, and D. Besozzi, "The impact of particles initialization in pso: parameter estimation as a case in point," in *2015 IEEE Conference on Computational Intelligence in Bioinformatics and Computational Biology (CIBCB)*, pp. 1–8, IEEE, 2015.
- [41] H. T. Rauf, W. H. Bangyal, J. Ahmad, and S. A. Bangyal, "Training of artificial neural network using pso with novel initialization technique," in *2018 International Conference on Innovation and Intelligence for Informatics, Computing, and Technologies (3ICT)*, pp. 1–8, IEEE, 2018.
- [42] D. H. Wolpert, "Stacked generalization," *Neural networks*, vol. 5, no. 2, pp. 241–259, 1992.
- [43] G. Huang, Y. Li, G. Pleiss, Z. Liu, J. E. Hopcroft, and K. Q. Weinberger, "Snapshot ensembles: Train 1, get m for free," *arXiv preprint arXiv:1704.00109*, 2017.